

Review of Hydraulic Roughness Scales in the Fully Rough Regime

Karen A. Flack
Department of Mechanical Engineering,
United States Naval Academy,
Annapolis, MD 21402
e-mail: flack@usna.edu

Michael P. Schultz
Department of Naval Architecture and Ocean
Engineering,
United States Naval Academy,
Annapolis, MD 21402
e-mail: mschultz@usna.edu

A review of predictive methods used to determine the frictional drag on a rough surface is presented. These methods utilize a wide range of roughness scales, including roughness height, pitch, density, and shape parameters. Most of these scales were developed for regular roughness, limiting their applicability to predict the drag for many engineering flows. A new correlation is proposed to estimate the frictional drag for a surface covered with three-dimensional, irregular roughness in the fully rough regime. The correlation relies solely on a measurement of the surface roughness profile and builds on previous work utilizing moments of the surface statistics. A relationship is given for the equivalent sandgrain roughness height as a function of the root-mean-square roughness height and the skewness of the roughness probability density function. Boundary layer similarity scaling then allows the overall frictional drag coefficient to be determined as a function of the ratio of the equivalent sandgrain roughness height to length of the surface.

[DOI: 10.1115/1.4001492]

1 Introduction

The most important unresolved issue regarding surface roughness in fluids engineering practice is how frictional drag (for external flows) or pressure drop (for internal flows) relates to the particular roughness topography. In other words, which roughness length scales best typify a surface hydraulically? Researchers have been working on this problem since the early experimental work of Nikuradse [1] and Colebrook [2]. However, most previously proposed roughness scales, discussed in detail later in this paper, are not sufficiently robust and are valid only for regular roughness or for a limited range of roughness types. What is needed in engineering practice is some means of relating the rough surface waveform to its frictional drag. In recent years, direct numerical simulations (DNS) have further elucidated the understanding of the underlying flow physics on rough walls (e.g., Refs. [3–5]). To date, however, DNS computations have been limited to idealized roughness types at a limited Reynolds number range, making them incapable of resolving issues regarding appropriate scaling for irregular three-dimensional roughness. Therefore, the need for accurate predictive correlations in engineering practice remains.

One of the most commonly employed fluids engineering tools is the Moody [6] diagram. This useful diagram relates the pressure drop in a pipe to the relative roughness (i.e., the ratio of the roughness height to the pipe diameter) and the Reynolds number. Moody developed the diagram to be used for naturally occurring roughness based on the results of Colebrook [2] for smooth and rough pipe flow. However, recent results by Allen et al. [7] and Langelandsvik et al. [8] show that the Moody diagram significantly overestimates the pressure drop in the transitionally rough flow regime for honed and commercial steel pipes, respectively. This clearly indicates that the Colebrook roughness function used in the formulation of the Moody diagram may not be applicable to a wide range of roughness of engineering interest. Fortunately, from an engineering standpoint, the Moody diagram likely gives a conservative estimate of pressure drop for a given roughness in the transitionally rough regime.

A more important issue regarding the Moody diagram is defin-

ing the appropriate roughness length scale to use as the roughness height. The diagram was developed using the equivalent sandgrain roughness height k_s [1]. However, k_s for a generic roughness cannot be accurately assigned a priori and must be determined experimentally. The roughness values listed on the diagram for copper, galvanized steel, etc., were determined from fitting a roughness height to match a measured pressure drop from an experiment, or in other words, determining k_s . The question then is how the height listed on the diagram relates to a physical roughness length scale measured from surface topography. This is especially pertinent since many of the manufactured surfaces listed on the Moody diagram do not have a consistent roughness. For example, some surfaces are listed with a roughness height that spans an order of magnitude. Additionally, the equivalent sandgrain roughness height is unknown for numerous other surfaces of engineering interest. As a result, one can only expect to obtain accurate results using the Moody diagram if k_s is known for the surface of interest and the flow is fully rough.

The naval architecture community includes the effects of surface roughness (e.g., paint, corrosion, and fouling) in an allowance coefficient, which is added to the smooth surface friction and residual (wave making) resistance coefficients when determining the overall drag of a full scale ship [9]. The International Towing Tank Committee [10] adopted the allowance coefficient of Bowden and Davison [11] to be used with the 1978 ITTC performance prediction line for ship resistance. This coefficient is a function of the mean hull roughness, the average peak-to-trough roughness height measured over 50 mm sampling lengths on the hull surface, as compared with the ship length. This equation, however, is not an accurate hull roughness penalty predictor since it includes additional residual components of resistance prediction, including model scale effects [12]. Townsin et al. [13] provided a formula for predicting the roughness penalty based on the mean hull roughness and the Reynolds number. While the inclusion of a Reynolds number dependence allows for calculations in the transitionally rough regime, the roughness parameter is still only based on a simple measure of the roughness height and does not account for other roughness texture characteristics. These considerations, along with a lack of accurate hull roughness measurements, led the ITTC Specialist Committee on Powering Performance Prediction [12] to conclude in 2005 that the methods used to correct for hull roughness and fouling are of doubtful accuracy.

Computational fluid dynamics (CFD) has generally represented rough surfaces by a smooth surface with modified boundary conditions or near wall equations. Discrete roughness models include

Contributed by the Fluids Engineering Division of ASME for publication in the JOURNAL OF FLUIDS ENGINEERING. Manuscript received July 3, 2009; final manuscript received March 12, 2010; published online April 20, 2010. Assoc. Editor: James A. Liburdy.

This material is declared a work of the US government and is not subject to copyright protection in the United States. Approved for public release; distribution is unlimited.

roughness as an additional drag term in the near wall momentum equations. Using this approach, the effect of roughness is confined to the near wall mean flow, not influencing the outer layer turbulence. Alternately, roughness can be accounted for in the turbulence by modifying the eddy viscosity models [14]. In this approach, a wall offset is included in the mixing length model that produces a nonzero eddy viscosity at the wall. The mean flow log region extends to this new origin. The amount of wall offset is a function of an empirically determined hydraulic roughness length. For the two layer approach, the wall layer model is patched to the outer layer model by modifying the k boundary condition in the $k-\varepsilon$ model, and the ω boundary condition in the $k-\omega$ model [15]. In the fully rough regime, the proposed $k-\varepsilon$ [16] and $k-\omega$ [17] models do not require a wall function since the log layer extends all the way to the wall. The common feature of all the models is an empirically determined term to accurately account for the roughness. Predictive correlations for a wide range of rough surfaces would provide computational models the necessary roughness length scale.

The development of more accurate predictive correlations relies on a robust database of experimental results that have accurate frictional loss data and detailed surface topography information. The approach taken in the present research is to expand on previous work that uses statistical moments of the surface profile, including a wider range of three-dimensional roughness. Successful correlation of the momentum deficit due to roughness with surface statistics will provide a method of drag prediction based solely on the surface roughness topography.

2 Background

The velocity deficit due to roughness has been represented in a variety of ways, based on the smooth wall log-law profile. Equation (1) represents the effect of roughness by the roughness function ΔU^+ or the downward shift in the log-law profile

$$U^+ = \frac{1}{\kappa} \ln y^+ + B - \Delta U^+ \quad (1)$$

where κ is the von Kármán constant and B is the intercept for a smooth wall. This can also be recast into a relative roughness form, Eq. (2), where k is a measure of the roughness height.

$$U^+ = \frac{1}{\kappa} \ln \frac{y}{k} + B - \Delta U^+ + \frac{1}{\kappa} \ln k^+ \quad (2)$$

Atmospheric boundary layer analyses generally represent roughness by a roughness length scale y_0 , which matches the smooth wall log-law profile, as shown in Eq. (3). In this equation, d is the zero-plane displacement, or the distance below the top of the roughness where the mean flow is zero.

$$U^+ = \frac{1}{\kappa} \ln \left(\frac{y-d}{y_0} \right) \quad (3)$$

Equation (3) is only valid in the fully rough regime; thus y_0 is an alternate scale that is similar to the equivalent sandgrain roughness height k_s , forcing collapse to a single profile in the fully rough regime.

Figure 1 shows typical rough wall boundary layer profiles and the corresponding roughness functions. The results presented are from Flack et al. [18] for flows over sandgrain and mesh roughness. The roughness heights for these surfaces are a significant fraction of the boundary layer thickness, resulting in large roughness functions. Similar roughness functions are obtained for the mesh and sandgrain surfaces at approximately the same unit Reynolds number even though the roughness heights differ substantially. This indicates that the roughness height alone is not adequate to scale the momentum deficit resulting from surface roughness.

If the shapes of the mean profile in the overlap and outer region of the boundary layer are similar for smooth and rough walls, then

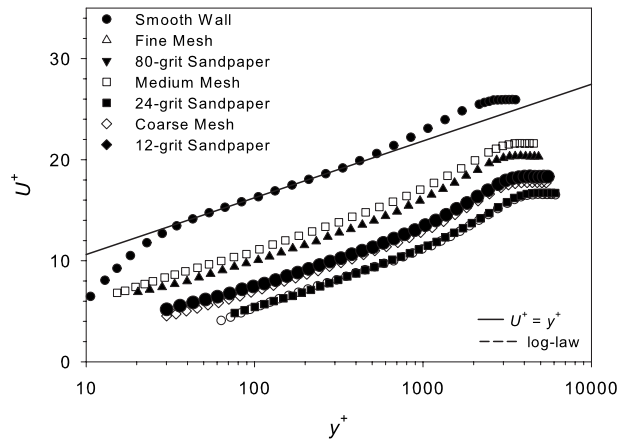


Fig. 1 Mean velocity profiles for mesh and sandpaper surfaces from Ref. [18]

the roughness function can also be expressed as the difference in skin friction for the smooth wall C_{fS} and the rough wall C_{fR} , at the same displacement thickness Reynolds number (Re_{δ^*}) as proposed by Hama [19] and shown in

$$\Delta U^+ = \left(\sqrt{\frac{2}{C_{fS}}} \right) - \left(\sqrt{\frac{2}{C_{fR}}} \right) = U_{eS}^+ - U_{eR}^+ \quad (4)$$

This allows roughness function results from rough surfaces obtained in the laboratory to be scaled up to full scale using the same outer layer similarity arguments. Mean flow similarity can be demonstrated through collapse of smooth and rough wall data when plotted in a velocity-defect form. Similarity has been experimentally verified by a number of researchers (e.g., Refs. [20–23]) including the present authors for a wide range of roughness types [18,24–28]. A representative velocity-defect plot from Flack et al. [18] for mesh and sandgrain roughness is shown in Fig. 2.

Ideally, the roughness function could be determined using a correlation based on a physical measure of the surface roughness instead of having to rely on laboratory hydrodynamic tests. The challenge is to determine the proper scales obtained from surface measurements that effectively correlate with the roughness function for a wide range of roughness types. Figure 3 shows the relationship between the roughness function and the roughness height for a variety of surfaces. For comparison, the uniform sandgrain roughness results of Nikuradse [1] are also presented. Three flow regimes are observed in Fig. 3. When the roughness Reynolds number k^+ is small, the flow is hydraulically smooth (i.e., $\Delta U^+=0$). In this case the perturbations generated by the roughness elements are completely damped out by the fluid vis-

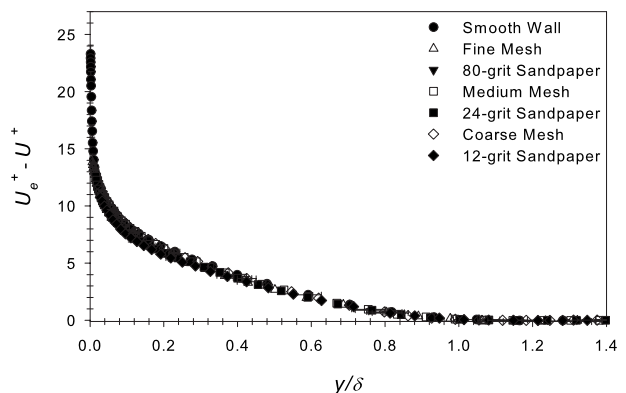


Fig. 2 Mean velocity profiles in velocity-defect form from Ref. [18]

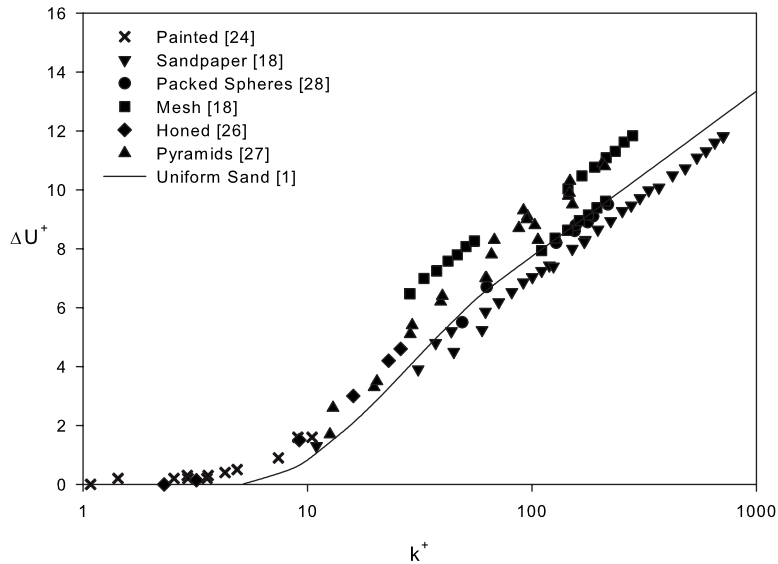


Fig. 3 Roughness function results for a variety of rough surfaces

cosity, creating no additional drag. As k^+ increases, the flow becomes transitionally rough. In the transitionally rough regime, viscosity is no longer able to damp out the turbulent eddies created by the roughness elements and form drag on the elements, as well as the viscous drag, contributes to the overall skin friction. As k^+ increases further, the roughness function reaches a linear asymptote. This asymptotic region at large values of k^+ is the fully rough regime. In this regime, the skin friction coefficient is independent of Reynolds number, and form drag on the roughness elements is the dominant mechanism responsible for the momentum deficit.

In Fig. 3, the peak-to-trough roughness height is used as the roughness scale. A common roughness scale in literature is the equivalent sandgrain roughness height k_s . This is the roughness height that produces the same roughness function as the uniform sandgrain of Nikuradse in the fully rough regime. Using the equivalent sandgrain roughness height as the roughness height in Eq. (2), and the log-law intercept for a uniform sandgrain surface

in relative roughness form ≈ 8.5 (Eq. (2)), k_s can be determined for a given roughness from its roughness function ΔU^+ in the fully rough regime using the following relationship:

$$B - \Delta U^+ + \frac{1}{\kappa} \ln k_s^+ = 8.5 \quad (5)$$

The equivalent sandgrain roughness height is then used as the scale in Fig. 4. As expected, all surfaces asymptote to the same line in the fully rough regime. It should be noted, however, that k_s^+ is unable to collapse the surfaces in the transitionally rough regime. Figures 3 and 4 highlight the fact that a single measure of the roughness height, i.e., k , k_s , and k_{rms} , is not able to collapse the roughness function results in all regimes for a range of surfaces.

A number of questions remain regarding the relationship between the roughness Reynolds number and the roughness function for a generic roughness. The value of k^+ (or k_s^+) when the surface

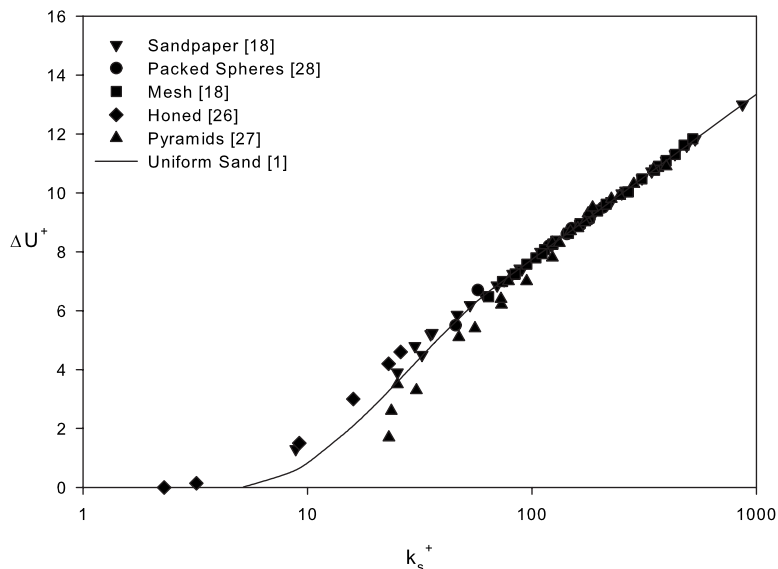


Fig. 4 Roughness function results for a variety of rough surfaces using k_s

roughness ceases to be hydraulically smooth has been shown to be a function of the roughness type. Second, the shape of the roughness function in the transitionally rough regime varies depending on the roughness type and is not known for most surfaces. Additionally, the value of k^+ that defines the onset of the fully rough regime is unknown for most roughness types. The transitionally rough regime has previously been defined as $5 < k_s^+ < 70$, based on the uniform sandgrain results of Nikuradse [1]. However, a wide range of values has been reported in literature for other roughness types. Ligrani and Moffat [29] reported that the transitionally rough regime spans $15 < k_s^+ < 50$ for a packed sphere bed. This range is reported as $3.5 < k_s^+ < 30$ for honed pipe roughness by Shockling et al. [30] and is given by the present authors [26] as $2.5 < k_s^+ < 25$ for a similar surface created by surface scratches. Langelandsvik et al. [8] indicated that the range of the transitionally rough regime is $1.4 < k_s^+ < 18$ for a commercial steel pipe. Lewkowicz and Musker [31] found that the onset of the fully rough regime ranged from $k_{rms}^+ = 17$ to 40 for ship-hull roughness. These disparate results for various roughness types clearly illustrate the difficulty of identifying scaling parameters that are applicable in both the transitionally and fully rough regimes. As illustrated in Fig. 4, collapse in the fully rough regime at high Reynolds numbers does not ensure that the transitionally rough regime has been properly captured. In fact, Clauser [32] discussed the difficulty of finding a roughness scale in the transitionally rough regime stating that some roughness types produce roughness functions with a monotonically changing slope while others have inflection points.

3 Previously Proposed Roughness Function Correlations

The development of correlations for the roughness function has been an area of active research for many years. Correlations range from simple models based on roughness height and pitch to more complicated relationships that include density and shape parameters, as detailed below.

Bettermann [33] proposed a functional relationship between the rough wall log-law intercept and a roughness spacing parameter λ , where $\lambda = \text{pitch}/\text{height}$ of 2D transverse bars, as shown in Eq. (6), for the range of λ listed.

$$f(\lambda) = B - \Delta U^+ + \frac{1}{\kappa} \ln k^+ = 17.35(1.165 \log_{10} \lambda - 1), \quad 1 \leq \lambda \leq 5 \quad (6)$$

Dvorak [34] modified this relationship, using a density parameter, $\lambda = \text{total surface area}/\text{total roughness area}$, which is equivalent to the spacing parameter of Bettermann for square bars. Dvorak added another relationship, which extends the range of applicability for more sparse roughness as follows:

$$f(\lambda) = 17.35(1.165 \log_{10} \lambda - 1) \quad 1 \leq \lambda \leq 4.68$$

$$f(\lambda) = -5.95(1.103 \log_{10} \lambda - 1) \quad \lambda > 4.68 \quad (7)$$

These correlations were developed using sandgrain surfaces [1,35,36], mesh screens [19], staggered rows of spheres [37], and square bars [33]. Simpson [38] modified the parameter further using $\lambda_k = \text{total surface area}/\text{total roughness frontal area}$ normal to the flow, showing reasonable agreement for spheres and cones [39], staggered hemispheres [40], and machined groves [41].

Dirling [42] introduced a combined density and shape parameter Λ . Roughness density is included as the ratio of the average element spacing d to roughness height k , whereas shape is accounted for in the frontal area of a single roughness element A_f and the windward wetted surface area of a single roughness element A_s .

$$\Lambda = \left(\frac{d}{k}\right) \left(\frac{A_f}{A_s}\right)^{-4/3} \quad (8)$$

Dirling provided correlations for the ratio of the equivalent sandgrain roughness height k_s , to roughness height k , for two-dimensional square rods, hemispheres, spheres, cones, right angles, as well as Nikuradse sand.

$$\frac{k_s}{k} = 0.0164\Lambda^{3.78}, \quad \Lambda \leq 4.93$$

$$\frac{k_s}{k} = 139\Lambda^{-1.90}, \quad \Lambda > 4.93 \quad (9)$$

Sigal and Danberg [43] introduced the effect of roughness density in a different manner, including S , the reference surface area before adding roughness, and S_f , the total frontal area of the roughness.

$$\Lambda_s = \left(\frac{S}{S_f}\right) \left(\frac{A_f}{A_s}\right)^{-1.6} \quad (10)$$

The following correlations were provided for two-dimensional transverse roughness including bars, rods, and ribs.

$$\frac{k_s}{k} = 0.00321\Lambda_s^{4.925}, \quad 1.400 \leq \Lambda_s \leq 4.890$$

$$\frac{k_s}{k} = 8, \quad 4.890 \leq \Lambda_s \leq 13.25$$

$$\frac{k_s}{k} = 151.711\Lambda_s^{-1.1379}, \quad 13.25 \leq \Lambda_s \leq 100 \quad (11)$$

van Rij et al. [44] expanded the use of this parameter to three-dimensional regular roughness, using the results of Schlichting [39] for staggered patterns of spheres, spherical segments, and cones. The data used incorporated the corrections given in Ref. [45]. The correlations for three-dimensional roughness are listed as follows:

$$\frac{k_s}{k} = 1.583 \times 10^{-5} \Lambda_s^{5.683}, \quad \Lambda_s < 7.842$$

$$\frac{k_s}{k} = 1.802\Lambda_s^{0.03038}, \quad 7.842 \leq \Lambda_s \leq 28.12$$

$$\frac{k_s}{k} = 255.5\Lambda_s^{-1.454}, \quad \Lambda_s > 28.12 \quad (12)$$

van Rij et al. [44] also tested irregular, three-dimensional roughness and applied a modified version of the roughness parameter, defined as

$$\Lambda_s = \left(\frac{S}{S_f}\right) \left(\frac{S_f}{S_s}\right)^{-1.6} \quad (13)$$

where S , S_f (as defined by Sigal and Danberg [43]), and S_s , the total windward wetted surface area, are calculated numerically based on detailed surface profiles. The equivalent sandgrain roughness is determined from the correlations developed for three-dimensional regular roughness, Eq. (12), using this modified roughness parameter and k_{avg} , the average roughness height. Experimental results for two rough surfaces were used to test the correlation: one completely covered by the roughness and one where rough regions of the surface alternate with smooth regions. The predicted skin friction, using the calculated values of k_s , compared well to experimentally results obtained from the pressure drop in a channel.

Additional three-dimensional roughness predictive correlations were presented by Waigh and Kind [46]. Their relationships were based on the results for a variety of roughness element shapes

including cubes, blocks, flat plates, cylinders, rods, cones, spheres, and hemispheres. They expressed the effect of roughness as a log-law shift C (Eq. (14)), using a similar form of the law of the wall as Eq. (2).

$$U^+ = \frac{1}{\kappa} \ln \frac{y}{k} + B - \Delta U^+ + \frac{1}{\kappa} \ln k^+ = \frac{1}{\kappa} \ln \frac{y}{k} + B - C \quad (14)$$

The element distribution is characterized by a density parameter Λ_k , which modifies the density parameter of Simpson [38] λ_k , with the streamwise aspect ratio k/s_m , where k is the roughness height and s_m is the streamwise roughness length.

$$\Lambda_k = \lambda_k \frac{k}{s_m} \quad (15)$$

The following relationships were presented for two density regimes:

$$C = 10.56 \log_{10} \left[\lambda_k \left(\frac{k}{b_m} \right)^{0.87} \left(\frac{A_w}{A_f} \right)^{0.44} \right] - 7.59, \quad \Lambda_k < 6$$

$$C = -5.75 \log_{10} \left[\lambda_k \left(\frac{k}{b_m} \right)^{0.55} \left(\frac{A_w}{A_f} \right)^{1.38} \right] + 5.78, \quad \Lambda_k > 6$$

(16)

where A_w is the roughness wetted area, A_f is the projected frontal area, and b_m is the spanwise roughness length. Waigh and Kind discussed the fact that the relationships were obtained for simple roughness element shapes in regular patterns and stressed the need to find ways to parametrize the geometry of natural roughness.

Turbine blade roughness that included surfaces with pitting, erosion, and deposits was studied by Bons [47]. Bons also adapted the Sigal and Danberg parameter for irregular roughness to calculate the equivalent sandgrain roughness for the surfaces as follows:

$$\log \left(\frac{k_s}{k} \right) = -1.31 \log(\Lambda_s) + 2.15 \quad (17)$$

The surface parameters were determined numerically from detailed surface profiles, with the roughness height k , taken as the average of the local peak-to-trough roughness height for smaller subregions. The skin friction correlation using k_s proposed by Schlichting [39] fits the experimental data best.

Many of the proposed correlations are valid for two- and three-dimensional regular roughnesses, including bars, blocks, cones, hemispheres, etc. Determining the required shape and density parameters for an idealized roughness is a relatively straightforward procedure. Extending this work to naturally occurring, irregular roughness is more challenging due to potentially complex surface features. While it is possible to determine the required shape and density parameters for irregular, three-dimensional roughness [44,47], complex numerical fitting procedures are needed. A simpler method of utilizing the surface topography map would be useful for predicting frictional drag due to roughness in a wider range of engineering applications.

Correlations that relate the statistical moments of the surface profile with the frictional drag or roughness function have been offered by various investigators. Musker [48] proposed an effective roughness height to correlate the roughness function $\Delta U^+ = f(k^+)$, as shown in

$$k^+ = \frac{k U_\tau}{\nu} = \frac{k_{rms} U_\tau}{\nu} (1 + a s_p) (1 + b s_k k_u) \quad (18)$$

where k_{rms} is the standard deviation, s_k is the skewness, k_u is the kurtosis of the surface elevation distribution, and s_p is the average slope of the roughness elements. The constants a and b were empirically chosen to collapse the data of naturally occurring surfaces. This effective roughness height was reasonably successful in collapsing the roughness function for pipes covered with posi-

tive replicas of ship-hull roughness. Musker cautioned that the cut-off wavelength used to characterize the surface should depend on the size of the roughness elements since the sizes of the turbulent eddies near the surface are a function of the longest surface wavelength. He proposed the use of the Taylor integral micro-scale [49] as the cut-off for the longest wavelength and two orders of magnitude lower for the smallest wavelengths.

Medhurst [50,51] reported correlations for painted ship roughness based on a parameter $C_1 h$, which he called the hydrodynamic roughness number, having units of roughness height. Medhurst used the following form of the roughness function:

$$\Delta U^+ = \frac{1}{\kappa} \ln \left[\frac{C_1 h U_\tau}{B_1 \nu} + C_2 \right] \quad (19)$$

where B_1 is found using an alternate form of the smooth wall log-law intercept

$$B = \frac{1}{\kappa} \ln[B_1] \quad (20)$$

Utilizing the linearized form of Eq. (20) along with experimental data, a regression analysis can be performed to determine $C_1 h$ and C_2 .

$$B_1 e^{\kappa \Delta U^+} = (C_1 h) \left(\frac{U_\tau}{\nu} \right) + B_1 C_2 \quad (21)$$

If the surface is assumed to follow a Colebrook form of the roughness function (i.e., monotonic), then $C_2 = 1.0$ and ΔU^+ is only a function of $C_1 h$. Medhurst presented different values of the hydrodynamic roughness number for three types of ablative paints. Medhurst also cautioned on the use of cut-off wavelengths and other filtering techniques, as well as spatial resolution issues that can bias results and reject important surface information.

Townsin and Dey [52] utilized the moments of the roughness amplitude energy spectral density, incorporating a variable long wavelength cut-off, to determine the roughness function for painted ship surfaces. The height of the roughness is represented by the spectral area m_0 , the slope by the second moment m_2 , and the range of frequencies composing the roughness profile by a bandwidth parameter $\alpha = m_0 m_4 / m_2^2$. Based on the results for 26 ship paint surfaces, the best correlation between the roughness function ΔU^+ and the roughness height k is shown in

$$k \propto \sqrt{\alpha m_0 m_2} = \sqrt{\frac{m_0^2 m_4}{m_2}} \quad (22)$$

While this technique shows promise, significant scatter was present using this correlation in the fully rough regime while the correlation did not collapse the data in the transitionally rough regime.

The correlations presented have demonstrated some utility in collapsing experimental data for a subset of rough surfaces, but they yield a high degree of variance when applied to a larger range of three-dimensional roughness types. Furthermore, many of the correlations are difficult to apply to irregular, three-dimensional roughness. The approach taken in the present research has been to expand on the previous work using statistical moments of the surface profile, including a wider range of three-dimensional roughness. Successful correlation of the roughness function with surface statistics will provide a method of drag prediction based solely on the surface roughness.

4 Full Scale Prediction Methods

Roughness function results for rough surfaces obtained in the laboratory can be scaled up to full scale using outer layer similarity arguments. Thus, knowing $\Delta U^+ = f(k^+)$ allows for the frictional drag of a full scale rough surface to be determined. If the equivalent sandgrain roughness k_s is taken as the roughness scale, then this functional relationship is valid for all roughness in the fully

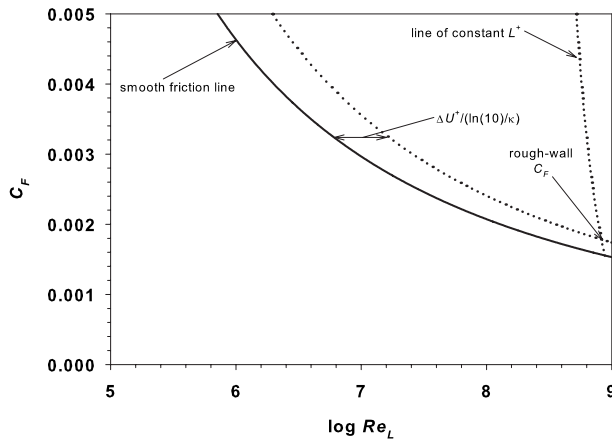


Fig. 5 Scaled-up procedure from C_F smooth to C_F rough

rough regime provided k_s is properly specified. Schultz [53] detailed the similarity methods used to determine the overall frictional resistance coefficient C_F for rough wall boundary layer flow over a flat plate of length L if the roughness function ΔU^+ is known. The methodology incorporates the analysis of Granville [54,55] and relies on outer layer similarity in the mean flow for smooth and rough walls, as demonstrated in the velocity-defect profiles shown in Fig. 2. A graphical representation of the scaling procedure is shown in Fig. 5. Here, the smooth wall overall frictional drag coefficient C_F is plotted as a function of $\log_{10}(\text{Re}_L)$ using the Karman-Schoenherr [56] friction line as follows:

$$\sqrt{\frac{2}{C_F}} = \frac{1}{\kappa} \ln(\text{Re}_L C_F) \quad (23)$$

The rough surface overall frictional resistance coefficient for a known roughness function is determined by displacing the smooth friction line by a distance $\Delta U^+ \kappa [\ln(10)]^{-1}$ in the positive $\log_{10}(\text{Re}_L)$ direction. For a given plate length L , a line of constant $L^+ = LU_\tau \nu^{-1}$, which satisfies the following relationship, is plotted:

$$\text{Re}_L = \frac{L^+}{\sqrt{\frac{C_F}{2} \left(1 - \frac{1}{\kappa} \sqrt{\frac{C_F}{2}} \right)}} \quad (24)$$

The intersection of this line and the rough surface line identifies C_F for the rough plate at a single value of Re_L for a given ΔU^+ .

If this process is repeated for a range of ΔU^+ and L , the overall frictional resistance coefficient can be mapped out. If the relationship $\Delta U^+ = f(k_s^+)$ is used to account for the roughness, then this diagram is valid for all roughness in the fully rough regime provided k_s is known. This is shown in Fig. 6, as a “Moody” type diagram, where the overall frictional drag coefficient is presented as function of the ratio of k_s to the overall length of the plate L . In the fully rough regime the relationship can be expressed as the following formula:

$$\sqrt{\frac{2}{C_F}} = -2.186 \ln\left(\frac{k_s}{L}\right) + 0.495 \quad (25)$$

With an estimated 10% uncertainty in ΔU^+ at 95% confidence, the resulting uncertainty in the overall frictional drag coefficient C_F is 2% for $k_s/L = 0.001$, decreasing to less than 1% for $k_s/L = 0.00001$.

On the diagram, it is assumed that the onset of the fully rough regime occurs at $k_s^+ = 70$, based on the uniform sandgrain results of Nikuradse. As noted previously, the onset of the fully rough regime is highly dependent on the specific roughness and likely occurs at lower values of k_s^+ for many types engineering roughness. Additional measurements that span the transitionally rough regime are needed to determine the important scales for predicting when a surface becomes fully rough. With the relationship given in Eq. (25), the frictional drag on a planar surface can be determined by identifying roughness scales that accurately predict k_s . It should also be noted that the roughness function could also be incorporated in CFD models and used to calculate the frictional drag of an arbitrary body covered with the given roughness.

5 Development of a New Roughness Correlation

The development of a roughness function correlation is restricted here to flows in the fully rough regime. In this regime, a larger number of experimental results are available, and it is possible to collapse all roughness functions to a single line if the equivalent sandgrain roughness height k_s is used as the roughness

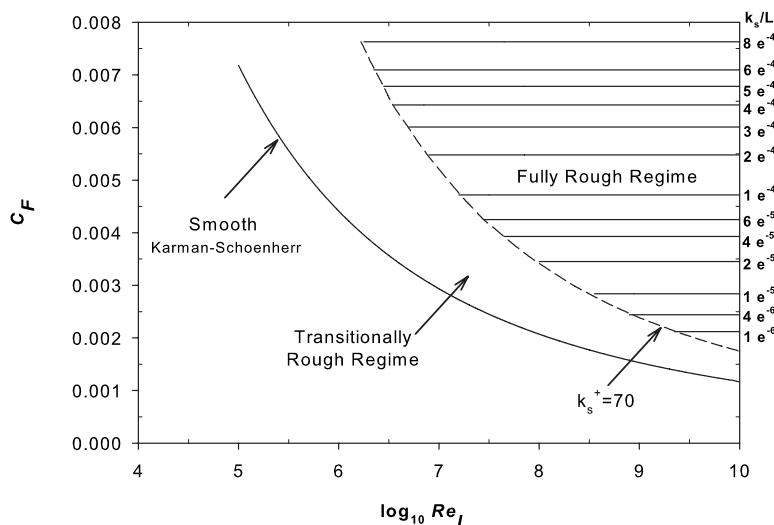


Fig. 6 Overall frictional drag coefficient in the fully rough regime

Table 1 Surfaces used in predictive correlation for k_s

| Surface | Ref. | k_r (μm) | k_{rms} (μm) | s_k | k_u | k_s actual (μm) | k_s predicted (μm) | % diff |
|--------------------------|------|----------------------------|---------------------------------------|--------|-------|-----------------------------------|--------------------------------------|--------|
| Sandpaper—80 grit | [18] | 546 | 67.9 | 0.497 | 4.49 | 529 | 522 | 1.3 |
| Sandpaper—24 grit | [18] | 1291 | 167 | 0.719 | 4.06 | 2626 | 1954 | 25.6 |
| Sandpaper—12 grit | [18] | 2466 | 320 | 1.51 | 6.17 | 6354 | 6512 | 2.5 |
| Packed spheres | [28] | 824 | 199 | 0.212 | 1.90 | 876 | 1146 | 30.8 |
| Packed spheres with grit | [28] | 738 | 158 | 0.315 | 2.22 | 1097 | 1018 | 7.2 |
| Honed (scratch) | [26] | 193 | 26.4 | -0.455 | 3.63 | 71.0 | 51.0 | 28.2 |
| Honed pipe | [30] | 15.96 | 2.5 | 0.31 | 4.05 | 7.5 | 16.0 | 113 |
| Commercial pipe | [8] | 27.27 | 5.0 | -0.19 | 2.53 | 8.0 | 16.5 | 106 |
| Gravel—medium | [23] | 3079 | 605 | 0.618 | 3.43 | 5383 | 5167 | 4.0 |
| Gravel—coarse | [23] | 7350 | 1490 | 0.0305 | 2.46 | 6785 | 6875 | 1.3 |
| Pyramid—A1 | [27] | 304.8 | 72.1 | 0.566 | 2.40 | 510 | 589 | 15.5 |
| Pyramid—A2 | [27] | 457.2 | 108 | 0.566 | 2.40 | 706 | 883 | 25.1 |
| Pyramid—A3 | [27] | 609.6 | 144 | 0.566 | 2.40 | 1301 | 1177 | 9.5 |
| Pyramid—B1 | [27] | 304.8 | 72.1 | 0.566 | 2.40 | 540 | 589 | 9.1 |
| Pyramid—B2 | [27] | 457.2 | 108 | 0.566 | 2.40 | 577 | 883 | 53.0 |
| Pyramid—B3 | [27] | 609.6 | 144 | 0.566 | 2.40 | 1012 | 1177 | 16.3 |

scale. This scale understandably has its limitations since it is not intrinsically related to roughness topography. The advantage of k_s is that it provides a “common currency” among different roughness types as pointed out by Bradshaw [57]. Here an investigation is made into which physical roughness scales, if any, effectively correlate with k_s . This study was conducted using the results from a variety of three-dimensional rough surfaces, listed in Table 1. Numerous other researchers have measured the roughness function in the fully rough regime for other surfaces. However, only results that also report detailed surface topographical measurements have been included.

A sample three-dimensional topographical map for the honed surface of Schultz and Flack [26] is shown in Fig. 7. This surface was profiled using a CyberOptics laser diode point range sensor laser profilometer system. The vertical accuracy of the sensor is 1 μm with a laser spot diameter of 10 μm . The data were digitized at increments of 25 μm in the lateral directions, and the sampling area was $5 \times 5 \text{ mm}^2$. The other surfaces of the present authors [18,24,27], as well as the surfaces of Castro [23], were profiled using the MicroPhotonics Nanavea ST300 white light chromatic aberration surface profilometer. The vertical accuracy of this system is 0.3 μm with a lateral resolution of 6 μm . Five replicate surface profiles were gathered on each of these surfaces as well as the surface shown in Fig. 7. The sampling interval was 25 μm , and the sampling length was 50 mm. The surface statistics and roughness parameters, listed in Table 1, were calculated

as the mean value from the replicate profiles. The data were not filtered to remove short or long wavelength roughness components. However, long wavelength or “wavy” roughness has not been included in this study. Expanding on the work of Napoli et al. [58], Schultz and Flack [27] determined that roughness with an effective slope ES less than approximately 0.35 does not scale on the roughness height. The relationship for the effective slope is shown in

$$ES = \frac{1}{L_s} \int_{L_s} \left| \frac{\partial r}{\partial x} \right| dx \quad (26)$$

Filtering, sampling interval, and sampling length can all have a significant effect on roughness statistics as pointed out by Medhurst [51] and Howell and Behrends [59]. This was not a primary focus in the present study. The practical difficulty in addressing the effect of these parameters is that not all surfaces were profiled using the same sampling interval and length. Specifying the most appropriate sampling interval, sampling length, and filtering length is quite complex and can be expected to depend at least to some extent on the inner and outer length scales of the flow in question. This point underlines the need for the adoption of a consistent method of measuring hydraulic surface roughness, as was highlighted by Howell and Behrends [59].

Common surface statistical parameters, as well as the wide

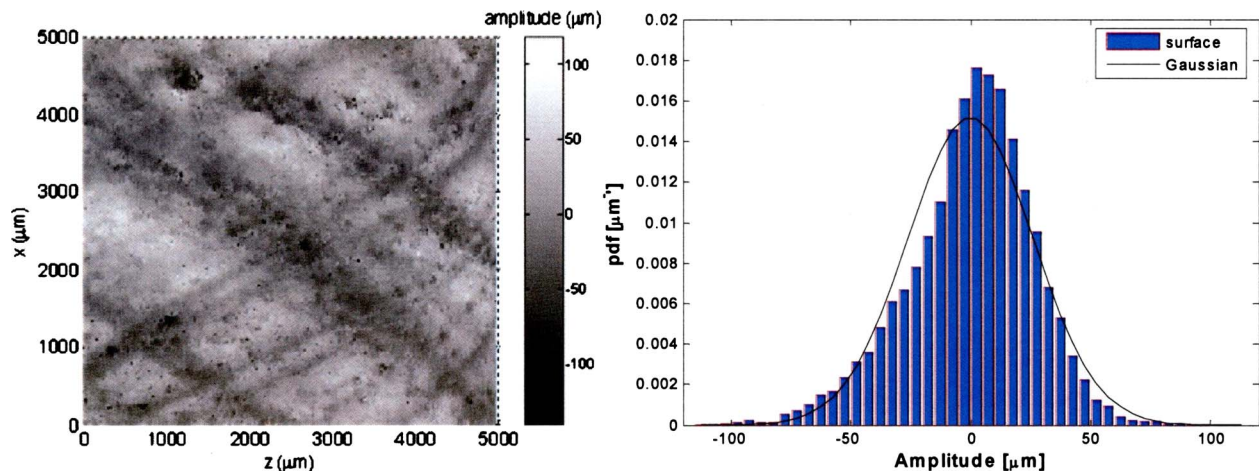


Fig. 7 Surface topography map and pdf of r , distance above the mean roughness elevation, for a honed surface

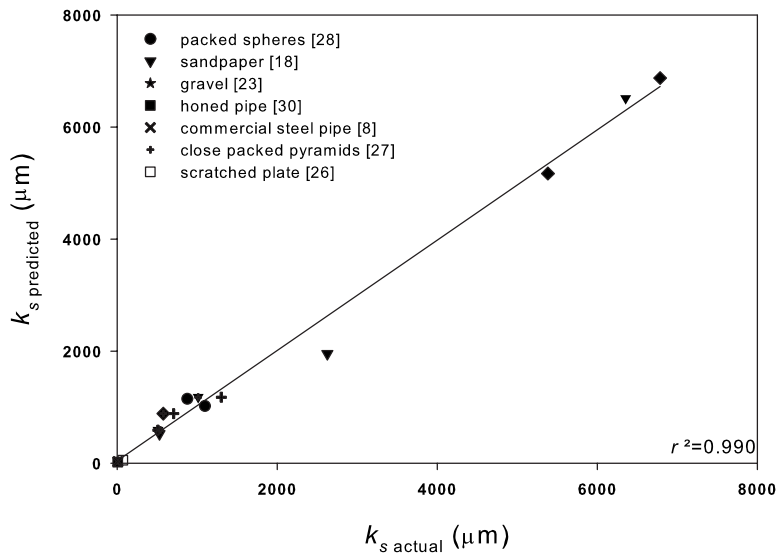


Fig. 8 Predicted k_s versus actual k_s using Eq. (27)

range of other roughness scaling parameters reviewed previously in this paper, were investigated as candidate hydraulic scales. This was done using a series of statistical correlations between the candidate hydraulic scales and the measured equivalent sandgrain roughness height k_s for the surface. This analysis indicated that the root-mean-square roughness height scale (k_{rms}) and the skewness of the roughness surface elevation probability density function (pdf) (s_k) had the strongest correlations with k_s . Based on this observation, it was decided to develop a single length-scale correlation using both of these parameters. A number of different functional forms were considered. The function that best correlates the present data (Table 1) is given in Eq. (27) and graphically represented in Fig. 8.

$$k_s = f(k_{rms}, s_k) \approx 4.43k_{rms}(1 + s_k)^{1.37} \quad (27)$$

In Fig. 8, k_s actual was determined using Eq. (8) for an experimentally determined value of ΔU^+ with $B=5.0$ and $\kappa=0.41$ in the fully rough regime. The surfaces used in this correlation along with some of their roughness statistics are shown in Table 1. The skewness is a quantitative way of describing whether the roughness has more peaks or valleys. A roughness with isolated large peaks will have a high positive skewness. Surfaces that have become rough due to deposits of roughness elements (i.e., exhaust particulates, biological fouling, etc.) will generally have positively skewed pdf's. A surface that is pitted (i.e., corrosion, surface wear, etc.) will have negatively skewed pdf's. It should be cautioned that only two surfaces used in the present correlation had a negative skewness, and both are relatively mild. The correlation, given in Eq. (27), has an additive constant of 1. This means that the present correlation would be undefined for $s_k \leq -1$. This constant was chosen in order to define a predictive correlation that is near the range of the parameter space that was investigated. It should be noted that using a larger additive constant would change the other constants in Eq. (27) but would not significantly reduce the goodness of fit. However, further data for surfaces with negative s_k are needed to validate and refine this correlation for a larger range of the parameter space. Nevertheless, Fig. 8 shows the linear correlation between the predicted value of k_s using the correlation and the measured k_s . The goodness of fit is excellent with $r^2=0.990$.

Table 1 also lists the difference between the measured and predicted values of the k_s . The correlation works very well for the sandgrain, sandpaper (gravel), and packed spheres covered with grit. This indicates that the correlation would do an excellent job of predicting the equivalent sandgrain roughness height for large

($k_s > 500 \mu\text{m}$) naturally occurring type roughness. The only exception is the 24 grit sandpaper surface. However, even with a 26% difference in the predicted k_s from the measured value for the 24 grit sandpaper, the predicted overall drag coefficient $C_F = 0.00773$ is only 6.5% in error from values measured in tow tank tests $C_F = 0.00826$ [60].

Considering the percent error from the expected value, the correlation does not adequately predict the small values of k_s for the honed and commercial steel pipes. This is not surprising due to the nature of the fitting where the sum of the square of the residual is being minimized. This will bias the best fit toward the larger roughness where the absolute value of the difference is larger even though the relative difference is smaller. Using the results of Shockling et al. [30], a 113% difference in the predicted value of k_s yields an error in friction factor of approximately 30%. Therefore, the correlation presented may not be adequate for all the roughness considered. However, it appears that the important scales for better predictive correlations are the root-mean-square roughness height and the skewness of the surface elevation pdf. It should be noted that this is a sparse data set to base a predictive correlation. Unfortunately, experimentally obtaining the roughness function for a single roughness requires a large number of boundary layer profile measurements. While pressure drop data are easier to obtain in pipe flow, it is more difficult to coat/manufacture the pipe surface with a specific roughness. Recent advances in computing the flow over complicated surfaces, which can be easily parametrically changed, may be capable of providing a larger data set covering more of the sample space. This should allow for improvement in predictive capabilities.

6 Conclusions and Recommendations

An investigation has been carried out to identify hydraulically relevant roughness scales for three-dimensional roughness in the fully rough regime. A range of common surface statistical parameters, as well as a host of roughness parameters from literature, was considered. The results indicate that the root-mean-square roughness height (k_{rms}) and the skewness of the surface elevation pdf (s_k) are the most effective parameters in describing a surface hydraulically. A correlation based on these parameters is offered, and it shows promising agreement with the measured equivalent sandgrain roughness height (k_s). However, further data are needed to validate and refine this correlation. Surfaces with negative s_k (i.e., pitted or eroded surfaces) would be especially helpful in this regard. Collapse of the roughness function in the fully rough re-

gime does not ensure collapse in the transitionally rough regime. In fact, the nonuniversal nature of the roughness function in the transitionally rough regime makes a universal scaling for this regime seem intractable. Therefore, the development of a Moody-type diagram that is applicable to a wide range of surfaces and is accurate in the transitionally rough regime appears highly unlikely.

Acknowledgment

The authors would like to thank the Office of Naval Research for financial support of this research. Thanks also go to Professor Ian Castro of the University of Southampton and Professor Lex Smits of Princeton University for providing surface samples, surface profiles, and data used in this research. Finally, the authors acknowledge the superior support given to this research by USNA Hydromechanics Laboratory and USNA Technical Support Branch.

Nomenclature

a = roughness function fitting constant
 A_f = frontal area of a single roughness element
 A_s = windward wetted area of a single roughness element
 A_w = wetted area of a single roughness element
 b = roughness function fitting constant
 b_m = spanwise roughness length
 B = smooth wall log-law intercept ≈ 5.0
 C = log-law shift in a relative roughness form
 C_f = skin friction coefficient $= \tau_w / \frac{1}{2} \rho U_e^2$
 C_F = frictional resistance coefficient $= F_D / \frac{1}{2} \rho U_e^2 S$
 $C_1 h$ = hydrodynamic roughness number
 C_2 = roughness function constant
 d = average roughness element spacing
 ES = effective roughness slope
 F_D = drag force
 k = arbitrary measure of roughness height
 k_{avg} = average roughness height
 k_{rms} = root-mean-square roughness
 height $= \sqrt{1/N \sum_{i=1}^N r_i^2}$
 k_s = equivalent sandgrain roughness height
 k_t = maximum peak-to-trough height $= r_{max} - r_{min}$
 k_u = kurtosis of the roughness elevation distribution
 $= (1/N) \sum_{i=1}^N r_i^4 / [(1/N) \sum_{i=1}^N r_i^2]^2$
 k_x = wavenumber of the surface roughness
 L = plate length
 L_s = sampling length
 m_0 = zeroth moment of the roughness amplitude energy spectra $= \int_0^\infty S_r dk_x$
 m_2 = second moment of the roughness amplitude energy spectra $= \int_0^\infty k_x^2 S_r dk_x$
 m_4 = fourth moment of the roughness amplitude energy spectra $= \int_0^\infty k_x^4 S_r dk_x$
 N = number of samples
 r = distance above the mean roughness elevation
 Re_{δ^*} = displacement thickness Reynolds number $= U_e \delta^* / \nu$
 Re_L = Reynolds number based on plate length $= U_e L / \nu$
 Re_θ = momentum thickness Reynolds number $= U_e \theta / \nu$
 s_k = skewness of the roughness elevation distribution $= (1/N) \sum_{i=1}^N r_i^3 / [(1/N) \sum_{i=1}^N r_i^2]^{3/2}$
 s_m = streamwise roughness length
 s_p = average roughness slope
 S = wetted surface area without roughness
 S_f = total frontal area of roughness
 S_r = energy spectral density of roughness elevation

U = mean velocity
 U_e = mean freestream velocity
 U_τ = friction velocity $= \sqrt{\tau_o} / \rho$
 y = normal distance from the wall or virtual origin
 y_0 = effective roughness height
 α = roughness bandwidth parameter $= m_0 m_4 / m_2^2$
 δ = boundary layer thickness
 δ^* = displacement thickness $= \int_0^\delta (1 - U/U_e) dy$
 ΔU^+ = roughness function
 κ = von Kármán constant ≈ 0.41
 λ = roughness spacing or density parameter
 λ_k = modified roughness density parameter
 Λ = roughness density and shape parameter
 Λ_k = modified roughness density parameter
 Λ_s = modified roughness density and shape parameter
 ν = kinematic viscosity of the fluid
 θ = momentum thickness $= \int_0^\delta U/U_e (1 - U/U_e) dy$
 τ_w = wall shear stress

Superscript

+ = inner variable (normalized with U_τ or U_τ / ν)

Subscript

min = minimum value
 max = maximum value
 R = rough surface
 S = smooth surface

References

- [1] Nikuradse, J., 1933, "Laws of Flow in Rough Pipes," NACA Technical Memorandum 1292.
- [2] Colebrook, C. F., 1939, "Turbulent Flow in Pipes, With Particular Reference to the Transitional Region Between Smooth and Rough Wall Laws," *J. Inst. Civ. Eng.*, **11**, pp. 133–156.
- [3] Flores, O., and Jiménez, J., 2006, "Effect of Wall-Boundary Disturbances on Turbulent Channel Flows," *J. Fluid Mech.*, **566**, pp. 357–376.
- [4] Lee, S. H., and Sung, H. J., 2007, "Direct Numerical Simulation of the Turbulent Boundary Layer Over a Rod-Roughened Wall," *J. Fluid Mech.*, **584**, pp. 125–146.
- [5] Orlandi, P., and Leonardi, S., 2008, "Direct Numerical Simulation of Three-Dimensional Turbulent Rough Channels: Parameterization and Flow Physics," *J. Fluid Mech.*, **606**, pp. 399–415.
- [6] Moody, L. F., 1944, "Friction Factors for Pipe Flow," *Trans. ASME*, **66**, pp. 671–684.
- [7] Allen, J. J., Shockling, M. A., and Smits, A. J., 2005, "Evaluation of a Universal Transitional Resistance Diagram for Pipes With Honed Surfaces," *Phys. Fluids*, **17**, p. 121702.
- [8] Langelandsvik, L. I., Kunkel, G. J., and Smits, A. J., 2008, "Flow in a Commercial Steel Pipe," *J. Fluid Mech.*, **595**, pp. 323–339.
- [9] 1988, *Principles of Naval Architecture*, Vol. II, E. V. Lewis, ed., Society of Naval Architects and Marine Engineers, Jersey City, NJ.
- [10] International Towing Tank Conference (ITTC), 1978, "Report of the Powering Performance Committee," 15th ITTC, Hague.
- [11] Bowden, B. S., and Davison, N. J., 1974, "Resistance Increments Due to Hull Roughness Associated With Form Factor Extrapolation Methods," National Physical Laboratory (NP) Ship Technical Manual 3800.
- [12] International Towing Tank Conference (ITTC), 2005, "Report of the Powering Performance Committee," 24th ITTC, Edinburgh, Scotland, UK.
- [13] Townsin, R. L., Byrne, D., Svensen, T. E., and Milne, A., 1981, "Estimating the Technical and Economic Penalties of Hull and Propeller Roughness," *Trans. SNAME*, **89**, pp. 295–318.
- [14] Durbin, P. A., 2009, "Limiters and Wall Treatments in Applied Turbulence Modeling," *Fluid Dyn. Res.*, **41**, p. 012203.
- [15] Leighton, R. I., and Walker, D. T., 2007, "Reynolds Stress Modeling for Rough Wall Turbulence: An Invited Paper," 37th AIAA Fluid Dynamics Conference and Exhibit, AIAA Paper No. 2007-4615.
- [16] Durbin, P. A., Medic, G., Seo, J. M., Eaton, J. K., and Song, S., 2001, "Rough Wall Modification of Two-Layer $k-\epsilon$," *ASME J. Fluids Eng.*, **123**, pp. 16–21.
- [17] Seo, J. M., 2004, "Closure Modeling and Numerical Simulation for Turbulent Flows: Wall Roughness Model, Realizability and Turbine Blade Heat Transfer," Ph.D. thesis, Stanford University, Stanford, CA.
- [18] Flack, K. A., Schultz, M. P., and Connelly, J. S., 2007, "Examination of a Critical Roughness Height for Boundary Layer Similarity," *Phys. Fluids*, **19**, p. 095104.
- [19] Hama, F. R., 1954, "Boundary-Layer Characteristics for Smooth and Rough Surfaces," *Trans. SNAME*, **62**, pp. 333–351.

- [20] Bandyopadhyay, P. R., 1987, "Rough Wall Turbulent Boundary Layers in the Transition Regime," *J. Fluid Mech.*, **180**, pp. 231–266.
- [21] Raupach, M. R., Antonia, R. A., and Rajagopalan, S., 1991, "Rough Wall Turbulent Boundary Layers," *Appl. Mech. Rev.*, **44**, pp. 1–25.
- [22] Antonia, R. A., and Krogstad, P. Å., 2001, "Turbulence Structure in Boundary Layers Over Different Types of Surface Roughness," *Fluid Dyn. Res.*, **28**, pp. 139–157.
- [23] Castro, I. P., 2007, "Rough-Wall Boundary Layers: Mean Flow Universality," *J. Fluid Mech.*, **585**, pp. 469–485.
- [24] Schultz, M. P., and Flack, K. A., 2003, "Turbulent Boundary Layers Over Surfaces Smoothed by Sanding," *ASME J. Fluids Eng.*, **125**, pp. 863–870.
- [25] Flack, K. A., Schultz, M. P., and Shapiro, T. A., 2005, "Experimental Support for Townsend's Reynolds Number Similarity Hypothesis on Rough Walls," *Phys. Fluids*, **17**, p. 035102.
- [26] Schultz, M. P., and Flack, K. A., 2007, "The Rough-Wall Turbulent Boundary Layer From the Hydraulically Smooth to the Fully Rough Regime," *J. Fluid Mech.*, **580**, pp. 381–405.
- [27] Schultz, M. P., and Flack, K. A., 2009, "Turbulent Boundary Layers on a Systematically-Variied Rough Wall," *Phys. Fluids*, **21**, p. 015104.
- [28] Schultz, M. P., and Flack, K. A., 2005, "Outer Layer Similarity in Fully Rough Turbulent Boundary Layers," *Exp. Fluids*, **38**, pp. 328–340.
- [29] Ligrani, P. M., and Moffat, R. J., 1986, "Structure of Transitionally Rough and Fully Rough Turbulent Boundary Layers," *J. Fluid Mech.*, **162**, pp. 69–98.
- [30] Shockling, M. A., Allen, J. J., and Smits, A. J., 2006, "Roughness Effects in Turbulent Pipe Flow," *J. Fluid Mech.*, **564**, pp. 267–285.
- [31] Lewkowicz, A. K., and Musker, A. J., 1978, "The Surface Roughness on Ship Hulls: Interaction in the Viscous Sublayer," *Proceedings of the International Symposium on Ship Viscous Resistance-SSPA*, Goteborg, Sweden.
- [32] Clauser, F. H., 1956, "The Turbulent Boundary Layer," *Adv. Appl. Mech.*, **4**, pp. 1–51.
- [33] Bettermann, D., 1965, "Contribution à l'étude de la Couche Limite Turbulente le Long de Plaques Rugueuses," *Center National de la Recherche Scientifique*, Report No. 65-6.
- [34] Dvorak, F. A., 1969, "Calculation of Turbulent Boundary Layers on Rough Surfaces in Pressure Gradients," *AIAA J.*, **7**, pp. 1752–1759.
- [35] Granville, P. S., 1958, "The Frictional Resistance and Turbulent Boundary Layer of Rough Surfaces," *J. Ship. Res.*, **2**, pp. 52–74.
- [36] Lui, C. K., Kline, S. J., and Johnston, J. P., 1966, "An Experimental Study of Turbulent Boundary Layers on Rough Walls," *Department of Mechanical Engineering, Stanford University*, Report No. MD-15.
- [37] Schlichting, H., 1937, "Experimental Investigation of the Problem of Surface Roughness," *NACA Technical Memorandum* 823.
- [38] Simpson, R. L., 1973, "A Generalized Correlation of Roughness Density Effects on the Turbulent Boundary Layer," *AIAA J.*, **11**, pp. 242–244.
- [39] Schlichting, H., 1979, *Boundary-Layer Theory*, 7th ed., McGraw-Hill, New York.
- [40] Chen, D. K., and Roberson, J. A., 1971, "The Structure of Turbulence in the Wakes of Roughness Elements," *ASCS Hydraulics Division Specialty Conference*, University of Iowa, Iowa City, IA.
- [41] Streeter, V. L., 1936, "Frictional Resistance in Artificially Roughened Pipes," *Proceedings of the ASCE*, Vol. 101, pp. 681–713.
- [42] Dirling, R. B., 1973, "A Method for Computing Rough Wall Heat Transfer Rates on Re-Entry Noses," *AIAA Paper No. 73-763*.
- [43] Sigal, A., and Danberg, J. E., 1990, "New Correlation of Roughness Density Effects on the Turbulent Boundary Layer," *AIAA J.*, **28**, pp. 554–556.
- [44] van Rij, J. A., Belnap, B. J., and Ligrani, P. M., 2002, "Analysis and Experiments on Three-Dimensional, Irregular Surface Roughness," *ASME J. Fluids Eng.*, **124**, pp. 671–677.
- [45] Coleman, H. W., Hodges, B. K., and Taylor, R. P., 1984, "A Re-Evaluation of Schlichting's Surface Roughness Experiment," *ASME J. Fluids Eng.*, **106**, pp. 60–65.
- [46] Waigh, D. R., and Kind, R. J., 1998, "Improved Aerodynamic Characterization of Regular Three-Dimensional Roughness," *AIAA J.*, **36**, pp. 1117–1119.
- [47] Bons, J. P., 2002, " St and C_F Augmentation for Real Turbine Roughness With Elevated Freestream Turbulence," *ASME Paper No. GT-2002-30198*.
- [48] Musker, A. J., 1980–1981, "Universal Roughness Functions for Naturally-Occurring Surfaces," *Trans. Can. Soc. Mech. Eng.*, **1**, pp. 1–6.
- [49] Taylor, G. I., 1938, "The Spectrum of Turbulence," *Proc. R. Soc. London, Ser. A*, **164**, pp. 476–490.
- [50] Medhurst, J. S., 1989, "The Systematic Measurement and Correlation of the Frictional Resistance and Topography of Ship Hull Coatings, With Particular Reference to Ablative Antifouling," Ph.D. thesis, University of Newcastle-upon-Tyne, Newcastle, UK.
- [51] Medhurst, J. S., 1990, "Outline of a Draft International Standard for the Measurement and Characterisation of Roughness Topography in Fluid Flow," *Proceedings of the RINA International Workshop on Marine Roughness and Drag*, London, UK.
- [52] Townsin, R. L., and Dey, S. K., 1990, "The Correlation of Roughness Drag With Surface Characteristics," *Proceedings of the RINA International Workshop on Marine Roughness and Drag*, London, UK.
- [53] Schultz, M. P., 2007, "Effects of Coating Roughness and Biofouling on Ship Resistance and Powering," *Biofouling*, **23**, pp. 331–341.
- [54] Granville, P. S., 1978, "Similarity-Law Characterization Methods for Arbitrary Hydrodynamic Roughness," *David W. Taylor Naval Ship Research and Development Center*, Report No. 78-SPD-815-01.
- [55] Granville, P. S., 1987, "Three Indirect Methods for the Drag Characterization of Arbitrarily Rough Surfaces on Flat Plates," *J. Ship. Res.*, **31**, pp. 70–77.
- [56] Schoennerr, K. E., 1932, "Resistances of Flat Surfaces Moving Through a Fluid," *Trans. SNAME*, **40**, pp. 279–313.
- [57] Bradshaw, P., 2000, "A Note on 'Critical Roughness Height' and 'Transitional Roughness'," *Phys. Fluids*, **12**, pp. 1611–1614.
- [58] Napoli, E., Armenio, V., and DeMarchis, M., 2008, "The Effect of the Slope of Irregularly Distributed Roughness Elements on Turbulent Wall-Bounded Flows," *J. Fluid Mech.*, **613**, pp. 385–394.
- [59] Howell, D., and Behrends, B., 2006, "A Review of Surface Roughness in Antifouling Coatings Illustrating the Importance of Cutoff Length," *Biofouling*, **22**, pp. 401–410.
- [60] Shapiro, T. A., Schultz, M. P., and Flack, K. A., 2004, "The Effect of Surface Roughness on Hydrodynamic Drag and Turbulence," *USNA Trident Scholar*, Report No. USNA-1531-2.